J. Fluid Mech. (1989), *vol.* 201, *pp.* 507–523
Printed in Great Britain

Nonlinear oscillatory convection in the presence of a vertical magnetic field

By R. M. CLEVER AND F. H. BUSSE
Institute of Geophysics and Planetary Physics, University of California at Los Angeles, CA 90024, USA
and Institute of Physics, University of Bayreuth, D-8580 Bayreuth, FRG

(Received 11 December 1987 and in revised form 11 October 1988)

Convection rolls in a fluid layer heated from below become unstable to disturbances in the form of waves travelling along the axis of the rolls when the Rayleigh number exceeds a critical value R_{II}. This transition to a time-dependent form of convection also occurs in the presence of a vertical magnetic field when the fluid is electrically conducting. In this paper the finite-amplitude properties of these waves are investigated for the values 0.1 and 0.025 of the Prandtl number. It is shown that the onset of oscillations reduces the heat transport by convection and that a mean flow in the direction of propagation is associated with the waves. Although the magnetic field has an inhibiting influence on steady convection, the inhibiting influence on the onset of oscillations is even stronger such that in some cases a higher heat transport is obtained in the presence of a magnetic field than in its absence. For similar reasons subcritical finite-amplitude onset of travelling-wave convection occurs for sufficiently large magnetic field strengths. Finally the stability of travelling-wave convection is investigated and the Rayleigh number R_{III} for the transition to asymmetric wave convection is determined.

1. Introduction

One of the most interesting features of convection in a fluid layer heated from below is the oscillations that occur when the Prandtl number has values of the order unity or less. These oscillations assume the form of waves which travel along the horizontal axis of the convection rolls and which manifest themselves as a periodic transverse shift of the convection rolls. These waves are characterized by a strong vertical vorticity which vanishes for steady two-dimensional rolls. The simplest theory of the onset of the oscillations is obtained in the limit of vanishing Prandtl number with stress-free boundary conditions (Busse 1972). The analytical expressions clearly show that the frequency ω of the oscillations is related to the circulation velocity of convection and the vertical vorticity is connected with the periodic transverse displacement of the rolls. In recent years the finite-amplitude properties of the waves and their stability have been explored. A systematic study of the dependence of these properties on the Prandtl number is described in the paper by Clever & Busse (1987) which contains references to related earlier work and which will be referred to in the following by CB. The present paper describes an extension of this work to the case when the fluid is electrically conducting and a vertical magnetic field is imposed.

Convection in the presence of a magnetic field has been studied for a long time (see, for example, Chandrasekhar 1961) because of its importance in stars and in the

metallic cores of planets. More recently magnetic fields have been introduced in convection experiments in order to obtain an extra control parameter which can be easily varied (Libchaber, Fauvre & Laroche 1983; Fauve *et al.* 1984). But there have been relatively few studies of the finite-amplitude properties of convection in the presence of a magnetic field. We refer to the review article by Proctor & Weiss (1982) for a survey of the subject. The numerical analysis described in this paper is closely related to studies of steady convection rolls and their stability in the presence of a vertical field (Busse & Clever 1982). This paper will be referred to in the following by BC82. The stability boundaries of the convection rolls with respect to the oscillatory instability found in that study provides the starting point for the analysis of the finite-amplitude waves treated in this paper.

As in BC82 the limit of high magnetic diffusivity λ will be assumed which corresponds closely to the experimental situation since liquid metals typically have magnetic Prandtl numbers of the order of 10^{-7}. As a consequence the magnetic Reynolds number is vanishingly small and the main effect of the magnetic field is the increase in the dissipation of mechanical energy owing to Ohmic heating. It is thus not surprising that few novel dynamical phenomena are encountered in the presence of an imposed magnetic field and that the main effect of the latter is to increase the critical Rayleigh numbers for steady convection (except in the case of a horizontal field) and for the onset of oscillating convection rolls. There is a dual role, however, performed by the magnetic field. Since the magnetic field inhibits motion fluctuating in time even more than steady motions in the cases considered in this paper, the curious effect results that convection in the presence of a magnetic field may transport more heat at a given Rayleigh number than in its absence. Provided the magnetic field strength is sufficiently high we also find subcritical onset of finite-amplitude oscillatory convection. We did not find this phenomenon for low magnetic field strengths and we thus have not been able to confirm the prediction of this phenomenon by Fauve, Bolton & Brachet (1987) in the absence of a magnetic field.

We must mention an error that has affected some of the results in our previous work, CB. In that analysis the mean flow that is induced by travelling waves of finite amplitude in the direction parallel to the axis of the rolls was neglected erroneously. After the appropriate corrections had been made, it was found that the results for the case of air (Prandtl number $P = 0.71$) remained unchanged within the limits of numerical accuracy. But in the cases of smaller P, deviations in the plot of various quantities become noticeable. We thus are including the corrected results in the present paper. The mean flow along the axis of the rolls grows proportionally to the square of the amplitude of oscillations and does not seem to have been noticed in any previous work. Since simulations of high-Rayleigh-number convection have usually assumed Prandtl numbers of the order unity, it is not surprising that this effect has not been found earlier. With decreasing Prandtl number the mean flow effect increases rapidly in magnitude and should become observable in the laboratory under the appropriate conditions.

The paper starts with the formulation of the basic equations and an outline of the numerical methods in §2. In §3 we discuss the properties of the numerical solutions for symmetric travelling-wave convection. In §4 the transition to asymmetric waves is considered, and some concluding remarks are added in §5.

2. Mathematical formulation of the problem

We consider a horizontal fluid layer of thickness d which is permeated by a homogeneous vertical magnetic field with flux density B_0. The electrical conductivity of the fluid is sufficiently high such that the magnetic field tends to impede the motions of the fluid. But the magnetic diffusivity λ is not low enough for the magnetic Reynolds number to reach values of the order unity or larger. This situation is realized in typical laboratory experiments with liquid metals. It also applies to processes in planetary cores of sufficiently small scale.

In order to introduce a dimensionless description of the problem we use d as lengthscale, d^2/κ as timescale, $\kappa\nu/d^3\gamma g$ as the scale of the temperature and $B_0\kappa/\lambda$ as the scale for the magnetic field where the symbols κ, λ, ν, γ, g refer to the thermal diffusivity, the magnetic diffusivity, the kinematic viscosity, the coefficient of thermal expansion, and the acceleration of gravity respectively. The equations of motion in the Boussinesq approximation, the heat equation for the deviation θ of the temperature from the static distribution and the equation of magnetic induction in the magnetohydrodynamic approximation assume the form

$$P^{-1}\left(\frac{\partial}{\partial t}+\boldsymbol{u}\cdot\boldsymbol{\nabla}\right)\boldsymbol{u}=-\boldsymbol{\nabla}\pi+k\theta+\nabla^2\boldsymbol{u}+Q\frac{\kappa}{\lambda}\boldsymbol{B}\cdot\boldsymbol{\nabla}\boldsymbol{B}, \tag{2.1a}$$

$$\boldsymbol{\nabla}\cdot\boldsymbol{u}=0, \tag{2.1b}$$

$$\left(\frac{\partial}{\partial t}+\boldsymbol{u}\cdot\boldsymbol{\nabla}\right)\theta=R\boldsymbol{k}\cdot\boldsymbol{u}+\nabla^2\theta, \tag{2.1c}$$

$$\frac{\kappa}{\lambda}\left(\frac{\partial}{\partial t}+\boldsymbol{u}\cdot\boldsymbol{\nabla}\right)\boldsymbol{B}=\frac{\kappa}{\lambda}\boldsymbol{B}\cdot\boldsymbol{\nabla}\boldsymbol{u}+\nabla^2\boldsymbol{B}, \tag{2.1d}$$

where the Rayleigh number R, the Prandtl number P and the Chandrasekhar number Q are defined by

$$R\equiv\gamma(T_2-T_1)gd^3/\kappa\nu,\quad P=\nu/\kappa,\quad Q=B^2d^2/\rho_0\mu\lambda.$$

The temperatures T_1 and T_2 with $T_1<T_2$ are prescribed at the upper and lower rigid boundaries of the layer; ρ_0 and μ denote the density and the magnetic permeability of the fluid and the unit vector $\boldsymbol{k}$ is directed opposite to the direction of gravity. We shall use a Cartesian system of coordinates with the z-coordinate in the direction of $\boldsymbol{k}$ and the x-coordinate in the direction of the axis of the convection rolls.

Since the velocity field $\boldsymbol{u}$ and the magnetic field $\boldsymbol{B}$ are solenoidal vector fields, the general representation

$$\boldsymbol{u}=\boldsymbol{\nabla}\times(\boldsymbol{\nabla}\times\boldsymbol{k}\phi)+\boldsymbol{\nabla}\times\boldsymbol{k}\psi+U\boldsymbol{i}\equiv\delta\phi+\varepsilon\psi+U\boldsymbol{i}, \tag{2.2a}$$

$$\boldsymbol{B}=\frac{\lambda}{\kappa}\boldsymbol{k}+\delta h+\varepsilon g+G\boldsymbol{i} \tag{2.2b}$$

can be used, where $\boldsymbol{i}$ is the unit vector in the x-direction. Since we require that ϕ, ψ, h and g are bounded functions whose averages over the (x,y)-plane vanish, the mean flow component $U\boldsymbol{i}$ and the distortion of the mean magnetic field described by $G\boldsymbol{i}$ must be written separately. In doing so we are anticipating that a mean flow component or mean distortion of the magnetic field in the y-direction does not occur. By taking the z-components of the curl and of the (curl)^2 of the equation of motion

(2.1*a*) and by taking the z-components of (2.1*d*) and of its curl, four equations for the scalar variables ϕ, ψ, h, g can be obtained,

$$P^{-1}\left(\frac{\partial}{\partial t}\nabla^2\Delta_2\phi+\boldsymbol{\delta}\cdot(\boldsymbol{u}\cdot\nabla\boldsymbol{u})\right)=\nabla^4\Delta_2\phi-\Delta_2\theta+Q\boldsymbol{k}\cdot\nabla\nabla^2\Delta_2 h, \tag{2.3a}$$

$$P^{-1}\left(\frac{\partial}{\partial t}\Delta_2\psi+\boldsymbol{\varepsilon}\cdot(\boldsymbol{u}\cdot\nabla\boldsymbol{u})\right)=\nabla^2\Delta_2\psi+Q\boldsymbol{k}\cdot\nabla\Delta_2 g, \tag{2.3b}$$

$$\left(\frac{\partial}{\partial t}+\boldsymbol{u}\cdot\nabla\right)\theta=\nabla^2\theta-R\Delta_2\phi, \tag{2.3c}$$

$$-\nabla^2\Delta_2 h=\boldsymbol{k}\cdot\nabla\Delta_2\phi, \tag{2.3d}$$

$$-\nabla^2\Delta_2 g=\boldsymbol{k}\cdot\nabla\Delta_2\psi. \tag{2.3e}$$

As a fifth equation (2.3*c*) we have rewritten equation (2.1*c*). The operator Δ_2 denotes the horizontal Laplacian, $\Delta_2\equiv\nabla^2-(\boldsymbol{k}\cdot\nabla)^2$. Because we shall restrict the attention to the case $\kappa\ll\lambda$ we have neglected all terms in the equations multiplied by κ/λ. In addition we obtain the following equations for U and G by taking the average over the (x,y)-plane (indicated by a bar) of the x-components of (2.1*a*) and (2.1*d*):

$$\frac{\partial^2 U}{\partial z^2}-P^{-1}\frac{\partial}{\partial t}U+Q\frac{\partial G}{\partial z}=-P^{-1}\frac{\partial\overline{(\Delta_2\phi(\partial_{xz}\phi+\partial_y\psi))}}{\partial z}+\eta, \tag{2.3f}$$

$$\frac{\partial^2 G}{\partial z^2}+\frac{\partial U}{\partial z}=0, \tag{2.3g}$$

where the constant η denotes a possible mean pressure gradient in the x-direction. The limit of high magnetic diffusion, $\kappa\ll\lambda$, offers the advantage that h can be immediately eliminated from the problem by inserting (2.3*d*) into (2.3*a*). The elimination of the variable g is not quite as straightforward since the boundary conditions for the magnetic field have to be considered. In particular we shall focus on the case of rigid boundaries with perfect electrical and thermal conductivity,

$$\phi=\frac{\partial}{\partial z}\phi=\psi=\theta=\frac{\partial}{\partial z}g=0\quad\text{at}\quad z=\pm\tfrac{1}{2}. \tag{2.4}$$

For steady rolls the functions ψ and g vanish identically and the nature of the magnetic boundary conditions is irrelevant. But for three-dimensional solutions ψ and g do not vanish in general and the magnetic boundary conditions must be specified as soon as three-dimensional perturbations of the rolls are considered. The stability of rolls has been investigated in BC82. The oscillatory instability appeared as the most prominent feature in the case of small Prandtl numbers which is of primary interest for the applications of the theory. In the present paper we analyse the travelling-wave solutions which are induced by the oscillatory instability.

To obtain travelling-wave solutions of (2.3) together with boundary conditions (2.4) we expand the dependent variables into complete systems of functions satisfying the boundary conditions,

$$\phi=\sum_{lmn}\left[\hat{a}_{lmn}\cos l\alpha_x(x-ct)+a_{lmn}\sin l\alpha_x(x-ct)\right]\begin{Bmatrix}\sin m\alpha_y y\\ \cos m\alpha_y y\end{Bmatrix}g_n(z)$$

$$\equiv\sum_{lmn}(\hat{a}_{lmn}\hat{\boldsymbol{\Phi}}_{lmn}+a_{lmn}\boldsymbol{\Phi}_{lmn}), \tag{2.5a}$$

$$\theta = \sum_{lmn} [\hat{b}_{lmn} \cos l\alpha_x(x-ct) + b_{lmn} \sin l\alpha_x(x-ct)] \begin{Bmatrix} \sin m\alpha_y y \\ \cos m\alpha_y y \end{Bmatrix} \sin n\pi(z+\tfrac{1}{2})$$

$$\equiv \sum_{lmn} (\hat{b}_{lmn}\, \hat{\Theta}_{lmn} + b_{lmn}\, \Theta_{lmn}), \quad (2.5b)$$

$$\psi = \sum_{lmn} [\hat{c}_{lmn} \cos l\alpha_x(x-ct) + c_{lmn} \sin l\alpha_x(x-ct)] \begin{Bmatrix} \cos m\alpha_y y \\ \sin m\alpha_y y \end{Bmatrix} \sin n\pi(z+\tfrac{1}{2})$$

$$\equiv \sum_{lmn} (\hat{c}_{lmn}\, \hat{\Psi}_{lmn} + c_{lmn}\, \Psi_{lmn}). \quad (2.5c)$$

The indices l and m run through all non-negative integers while n runs through all positive integers. The functions $g_n(z)$ were introduced by Chandrasekhar (1961, p. 635) and have also been defined in equation (4*a*) of Clever & Busse (1974). As in CB the upper functions in the wavy brackets of (2.5) must be chosen for odd l, the lower functions for even l. For the given expansion (2.5*c*) for ψ, (2.3*e*) can be solved subject to the boundary condition (2.4) for g, with the result

$$g = \sum_{l,m,n} \left(\hat{c}_{lmn} \frac{\partial}{\partial z} \hat{\Psi}_{lmn} + c_{lmn} \frac{\partial}{\partial z} \Psi_{lmn} \right) (m^2\alpha_y^2 + l^2\alpha_x^2 + n^2\pi^2)^{-1}. \quad (2.6)$$

The distortion G of the mean field can be eliminated from the problem by integrating (2.3*f*) once. Using the expansion

$$U = \sum_n U_n \sin n\pi(z+\tfrac{1}{2}) \quad (2.7a)$$

for a stationary mean flow, we obtain as the equation for the coefficients U_n

$$U_n(n^2\pi^2 + Q) = -P^{-1} \sum_{lmpk} \Big\{ (\hat{a}_{lmp}\, a_{lmk} - \hat{a}_{lmk}\, a_{lmp})\, (l^2\alpha_x^2 + m^2\alpha_y^2)\, \tfrac{1}{2} l\alpha_x \int_{+\frac{1}{2}}^{-\frac{1}{2}} \sin n\pi(z+\tfrac{1}{2})$$

$$\times (g_p g_k')'\, \mathrm{d}z - (\hat{a}_{lmp}\, \hat{c}_{lmk} + a_{lmp}\, c_{lmk})\, (l^2\alpha_x^2 + m^2\alpha_y^2) \frac{m\alpha_y}{2} (-1)^l$$

$$\times \int_{-\frac{1}{2}}^{\frac{1}{2}} \sin n\pi(z+\tfrac{1}{2})\, (g_p \sin k\pi(z+\tfrac{1}{2}))'\, \mathrm{d}z \Big\} - \frac{4\eta}{\pi n} p(n), \quad (2.7b)$$

where the symbol $p(n)$ denotes zero for even n and unity for odd n.

After inserting (2.5), (2.6), (2.7*a*) into (2.3*a*, *b*, *c*), multiplying these equations with the functions $\hat{\Phi}_{ijk}$, Φ_{ijk}, $\hat{\Psi}_{ijk}$, Ψ_{ijk}, $\hat{\Theta}_{ijk}$, and Θ_{ijk} and averaging them over the fluid layer we obtain a system of nonlinear algebraic equations for the unknown coefficients $\hat{a}_{lmn}$ etc. We shall not give these equations explicitly here since they are similar to those used in earlier work, for example in Busse & Frick (1985). In order to solve them by a Newton–Raphson iteration method we must truncate them. As in CB we shall neglect all coefficients $\hat{a}_{ijk}$ etc. and corresponding equations for indices satisfying the truncation condition

$$i+j+k > N_T. \quad (2.8)$$

By changing N_T the quality of the approximate solution obtained through this truncation procedure can be checked. A useful criterion is that sensitive properties of the solution such as the convective heat transport do not change by more than 2 or 3% when N_T is replaced by $N_T - 1$. The computational work can be reduced by

using the property that only coefficients with even $l+k$ in (2.5a) and (2.5b) and with odd $l+k$ in (2.5c) are involved in the travelling-wave solution bifurcating from the solution in the form of rolls. Finally the phase speed c has to be determined in the course of the Newton–Raphson procedure. By requiring $a_{111} = 0$ we fix the phase of the travelling wave and thereby gain an extra equation which we use for the determination of c.

As outlined in CB the special form (2.5) of the travelling-wave solutions originates from the symmetry of the oscillatory instability. (Note that for ψ in CB the opposite of the selection rules mentioned below (2.4) of CB apply.) This form of the solution does not give rise to a Reynolds stress in the y-direction, but a finite mean flow in the x-direction can be generated. In the case of the travelling-wave solution bifurcating from the steady-roll solution this mean flow is symmetric about $z = 0$, i.e. only coefficients U_n with odd n contribute in (2.7a). When the horizontal extent of the convection layer is very large in comparison with its height, the development of the mean flow will not produce a counteracting pressure gradient and η can be set equal to zero. But in layers of finite aspect ratio the sidewalls are likely to exert a constraining influence in that a pressure gradient will be set up such that the mean flow averaged over the z-coordinate vanishes. We thus shall distinguish two cases of mean flow: the unrestricted case (u) with $\eta = 0$; and the restricted case (r) with η being determined by the condition

$$\int_{-\frac{1}{2}}^{\frac{1}{2}} U \,\mathrm{d}z = 0, \tag{2.9a}$$

$$\begin{aligned}\eta = -\left(\sum_n \left(\frac{2}{n\pi}\right)^2 (1-(-1)^n)\right)^{-1} \sum_{nlmpk} \Big\{ & (\hat{a}_{lmp}\, a_{lmk} - \hat{a}_{lmk}\, a_{lmp})\,(l^2\alpha_x^2 + m^2\alpha_y^2)\,\tfrac{1}{2} l \alpha_x \\ & \times \int_{-\frac{1}{2}}^{\frac{1}{2}} \sin n\pi(z+\tfrac{1}{2})\,(g_p\, g_k')'\,\mathrm{d}z - (\hat{a}_{lmp}\, \hat{c}_{lmk} + a_{lmp}\, c_{lmk})\,(l^2\alpha_x^2 + m^2\alpha_y^2)\,\frac{m\alpha_y}{2}(-1)^l \\ & \times \int_{-\frac{1}{2}}^{\frac{1}{2}} \sin n\pi(z+\tfrac{1}{2})\,(g_p \sin k\pi(z+\tfrac{1}{2}))'\,\mathrm{d}z \Big\} P^{-1}\frac{2}{n\pi}.\end{aligned} \tag{2.9b}$$

Fortunately, the differences between the two cases are relatively small in the region of the parameter space that has been investigated. For Prandtl numbers of the order unity or larger the mean flow given by (2.7) turns out to be so small that its neglect changes the results only imperceptibly. The results of CB for air thus remain unchanged within the line thickness of the relevant figures; but the results for $P = 0.1$ and for $P = 0.025$ require corrections, which are given in the following in the special case $Q = 0$.

3. Travelling-wave convection

One of the most remarkable features connected with the onset of travelling-wave convection are the substantial decreases in the slope of the convective heat transport as a function of the Rayleigh number at low Prandtl numbers. While the heat transport hardly differed for rolls and travelling-wave convection in the case $P =$ 0.71 of CB, the change in the slope of the Nusselt-number curve rapidly magnifies as the Prandtl number decreases, as can be seen from a comparison of figure 1 for $P =$ 0.1 and figure 2 for $P = 0.025$. In these figures the Nusselt number has been plotted

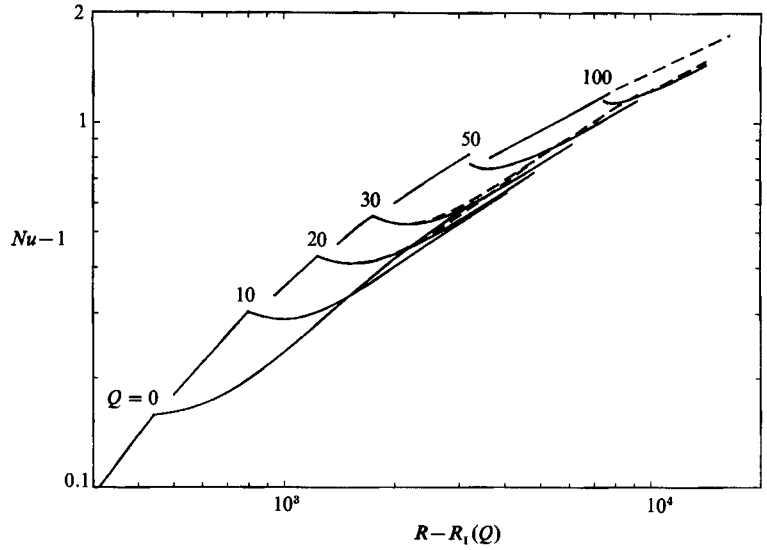

FIGURE 1. The Nusselt number Nu as a function of the Rayleigh number for different values of Q at $P = 0.1$. The combinations (2.6, 2.2, 0), (2.7, 2.5, 10), (2.8, 2.7, 20), (2.9, 2.8, 30), (3.1, 3.0, 50) and (3.3, 3.2, 100) have been used for (α_y, α_x, Q). The solid lines for two-dimensional convection rolls have been extended up to $R = R_{II}$. In the case $Q = 100$ this line has been extended by a dashed line. The Nusselt number for travelling-wave convection is given by a solid line in the restricted case (r) and by a dashed line in the unrestricted case (u).

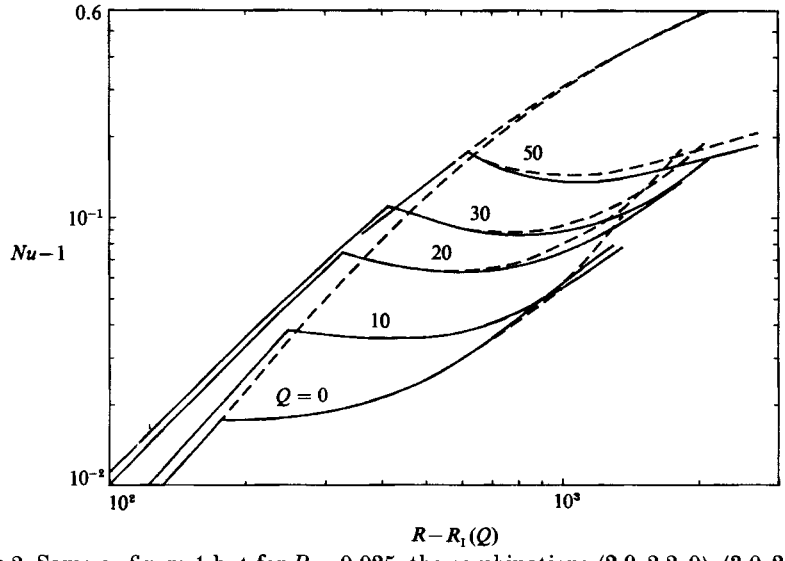

FIGURE 2. Same as figure 1 but for $P = 0.025$. the combinations (2.9, 2.2, 0), (3.0, 2.5, 10), (3.2, 2.7, 20), (3.3, 2.9, 30) and (3.4, 3.0, 50) have been used for (α_y, α_x, Q). In the cases $Q = 0$, $Q = 50$ the lines for two-dimensional convection rolls have been extended by dashed lines beyond the point of bifurcation.

for two-dimensional steady rolls and for three-dimensional travelling waves for various values of Q. At finite values of Q the change in slope becomes amplified such that an actual drop in the heat transport occurs.

In order to emphasize the general similarity of the curves, $R-R_I$ has been used as the abscissa, where R_I is the Rayleigh number for onset of convection, as a function

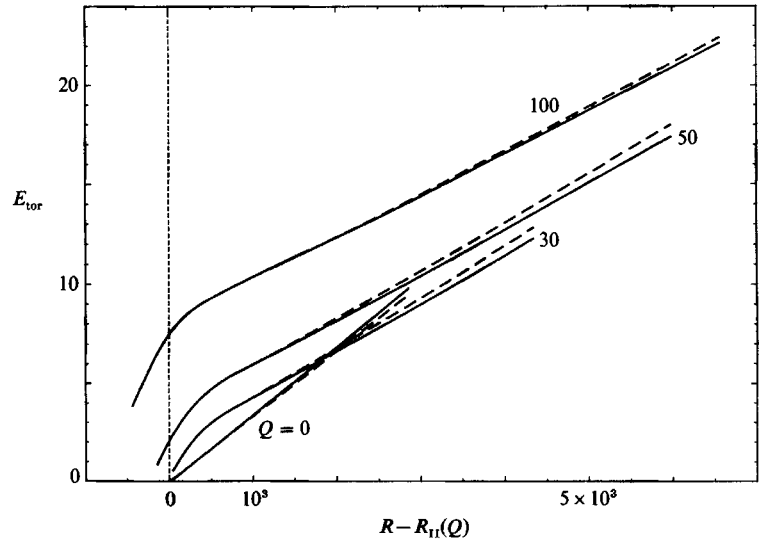

FIGURE 3. Kinetic energy of the toroidal component of motion, E_{tor}, as a function of the Rayleigh number for $P = 0.1$ and values of Q as indicated. The values of $(\alpha_y, \alpha_x, R_{II}, Q)$ are given by (2.6, 2.2, 2145, 0), (2.9, 2.8, 4158, 30), (3.1, 3.0, 6015, 50) and (3.9, 3.2, 11438, 100)

of Q and α_y (see, for example, figures 13 and 14). Because of the presence of the skewed varicose instability (BC82) a slightly smaller value than the critical value α_c has been chosen for α_y. This procedure seems reasonable also because wavelengths larger than the critical value are typically observed in experiments. The inhibiting influence of the magnetic field on the onset of oscillations is even more pronounced than the stabilizing influence on the onset of convection. As a result there are ranges where the convective heat transport in the presence of a vertical magnetic field is larger than in its absence. This possibility occurs for example in the case $P = 0.025$ for values of $Q \lesssim 30$ for Rayleigh numbers just below the onset of travelling waves.

As can be noticed in figure 1 the Nusselt-number curves exhibit a gap for the higher values of Q. This gap is caused by the subcritical onset of the travelling-wave solution. A plot of the kinetic energy connected with the toroidal component of motion described by ψ indicates this phenomenon more clearly, as shown in figure 3. While the toroidal component vanishes for two-dimensional rolls, it is a characteristic property of travelling wave convection. In fact, the increase in the toroidal kinetic energy

$$E_{tor} \equiv \tfrac{1}{2}\langle |\boldsymbol{k} \times \boldsymbol{\nabla}\psi|^2 \rangle \tag{3.1a}$$

and the concurrent decrease of the poloidal kinetic energy

$$E_{pol} \equiv \tfrac{1}{2}\langle |\boldsymbol{\nabla} \times (\boldsymbol{\nabla} \times \boldsymbol{k}\phi)|^2 \rangle \tag{3.1b}$$

explain the decrease in the convective heat transport since only the poloidal component of motion contributes to the convective heat transport.

In the case of the supercritical onset of travelling waves the toroidal kinetic energy grows approximately proportional to $R - R_{II}$ and a plot of (3.1a) divided by $R - R_{II}$ is more revealing. Figure 4 shows such a plot for $P = 0.025$. The plots of the poloidal kinetic energy (3.1b) shown in figures 5 and 6 resemble those of the Nusselt number.

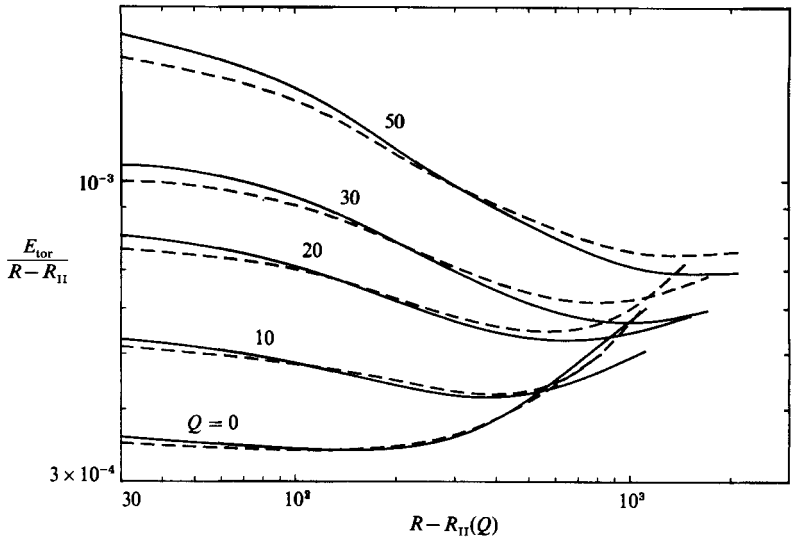

FIGURE 4. The quantity $E_{tor}/(R-R_{II})$ is displayed for the indicated values of Q for $P = 0.025$. The dashed lines indicate deviations for the unrestricted case (u). The same solutions have been used as in figure 2.

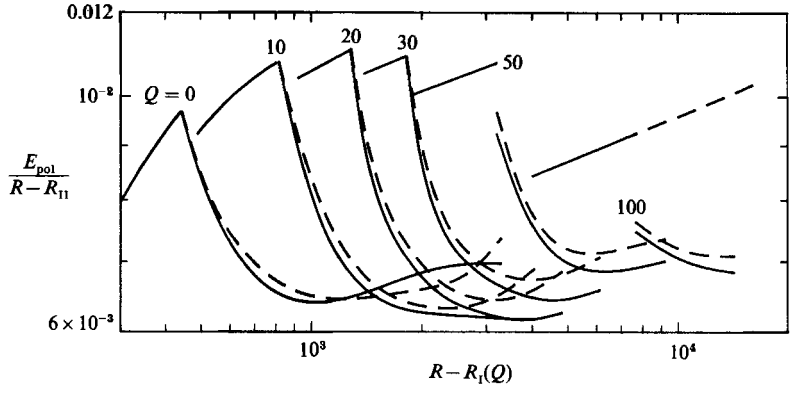

FIGURE 5. The kinetic energy of the poloidal component of motion E_{pol} is shown as function of the Rayleigh number for several values of Q for $P = 0.1$. The same solutions as in figure 1 have been used.

As mentioned above, the extraction of energy for the new degree of motion excited by the travelling-wave motion is responsible for the decreases in the poloidal kinetic energy. As in the case of the heat transport, the slope of the curves recovers and for large Rayleigh numbers the curves of three-dimensional convection tend to parallel those for the unstable two-dimensional convection rolls. For large Rayleigh numbers the convergence of the curves for different values of Q can be noted. The decrease of the circulation velocity in the rolls after the onset of instability also results in a decrease of the frequency of oscillation, as is evident from figures 7 and 8. In contrast to the quantities discussed above, the frequency shows a stronger influence of the mean flow conditions (2.9*a*). Since the mean flow is directed predominantly in the direction of the phase propagation of the travelling wave the frequency in the unrestricted case is larger than in the restricted case. At about the same place as where the Nusselt number and the poloidal kinetic energy resume their growth with

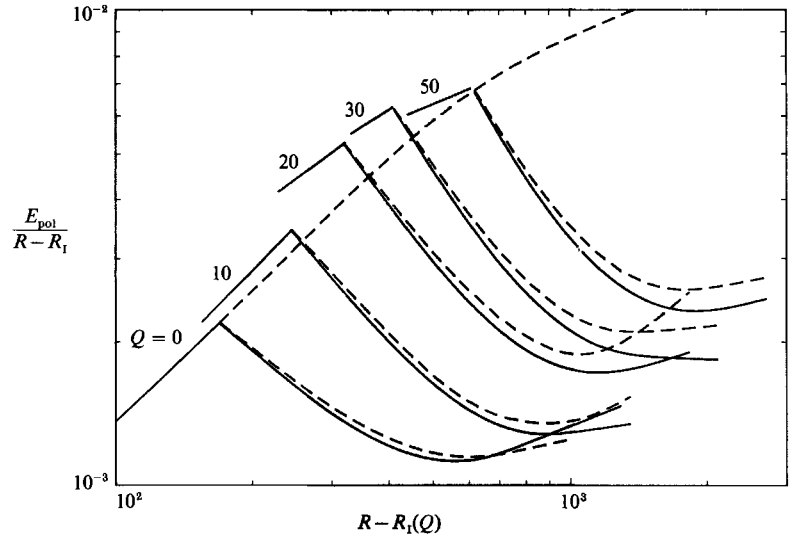

FIGURE 6. Same as figure 6 but for $P = 0.025$. The same solutions as in figure 2 have been used.

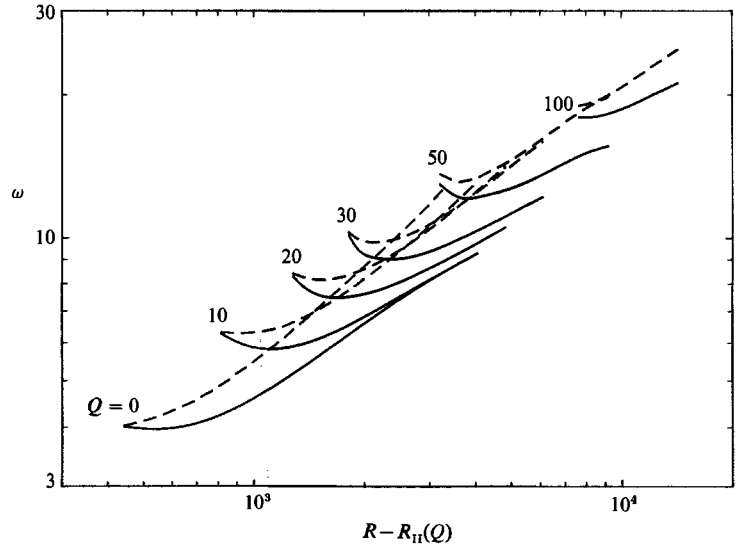

FIGURE 7. The frequency ω of oscillation as a function of the Rayleigh number for $P = 0.1$ for the same solutions that have been used in figure 1.

increasing Rayleigh number the frequency also starts to grow again. It will be of interest to find this non-monotonic dependence in experimental observations.

The general similarity of travelling-wave convection with and without the presence of a vertical magnetic field is reflected in the appearance of the motion. Here we show just two examples, in figures 9 and 10, which demonstrate this similarity. The plots shown in CB in the case $Q = 0$ are hardly changed within the accuracy of the plots by the inclusion of the mean flow terms and can still be used for comparisons. In the present figures also the temperature variation averaged over the depth of the layer and the streamlines of the toroidal component of the velocity field are shown for comparison. Because of the low Prandtl number, small-scale

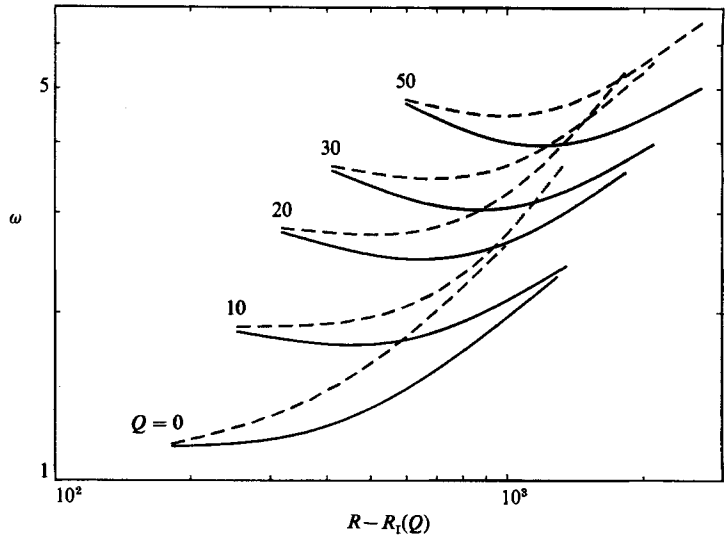

FIGURE 8. Same as figure 7 but for $P = 0.025$. The same solutions as in figure 2 have been employed.

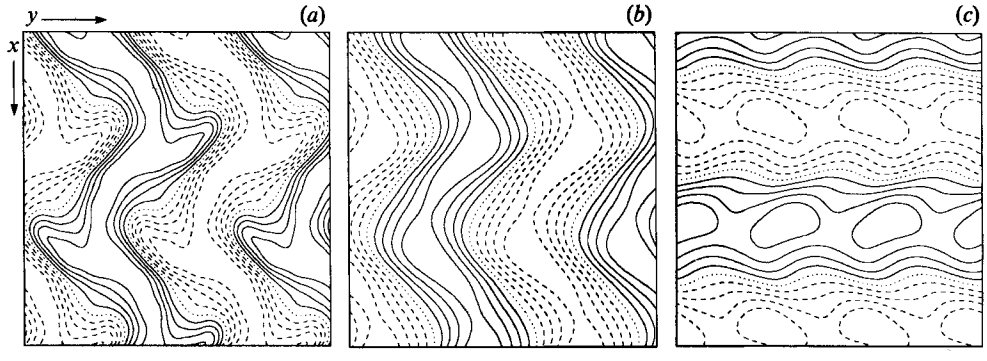

FIGURE 9. (*a*) Lines of constant vertical velocity at $z = 0$, $w = n^* w_{\max}/10$ for $n = -4, -3, \ldots, 4$; (*b*) lines of constant

$$\bar{\theta} \equiv \int_{-\frac{1}{2}}^{\frac{1}{2}} \theta \, \mathrm{d}z;$$

(*c*) lines of constant ψ. For (*a–c*) $P = 0.025$, $R = 4000$, $Q = 50$, $\alpha_y = 3.4$, $\alpha_x = 3.0$ with the restricted mean flow. Lines with negative n are dashed, the line $n = 0$ is dotted, lines with positive n are solid. The wave propagates in the negative x-direction.

contributions to the temperature field are more strongly damped than corresponding contributions to the velocity field. The temperature field not only looks much smoother than the vertical velocity, but the amplitude of the temperature wave is also slightly reduced. The transverse back and forth shifting of the rolls owing to the toroidal component of motion is clearly evident from the streamlines shown in part (*c*) of the figures. Part (*c*) also explains the hook-like evolution of the crest of the waves which is obviously related to the closed streamlines appearing in the toroidal field as the result of nonlinear interactions.

We finally consider the mean flow generated by the travelling-wave convection. In figures 11 and 12 the kinetic energy of the mean flow has been plotted for the two Prandtl-number cases. From the comparison with the results of figures 4–6 it is

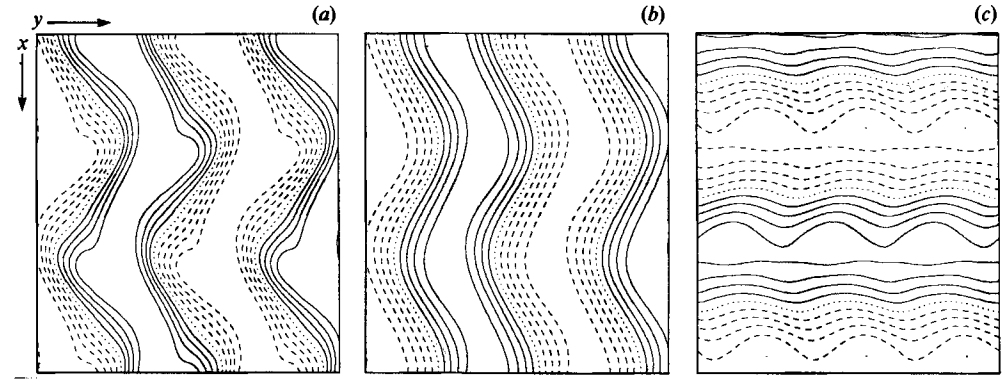

FIGURE 10. Same as figure 9, but for $P = 0.1$, $R = 8500$, $Q = 30$, $\alpha_y = 2.9$, $\alpha_x = 2.8$.

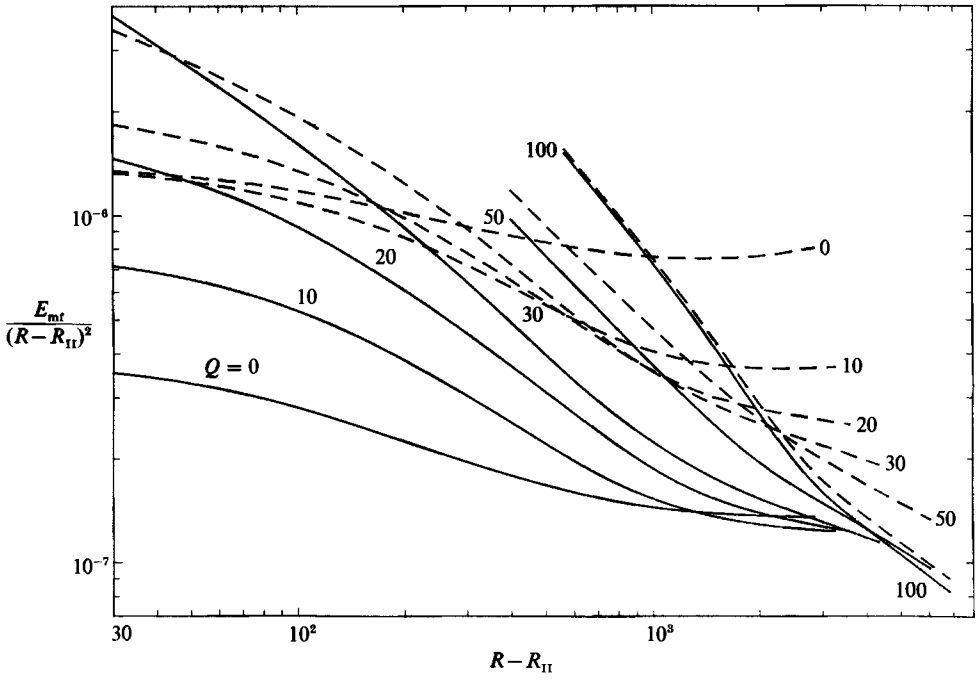

FIGURE 11. The kinetic energy of the mean flow in the restricted (solid lines) and unrestricted cases (dashed lines) for the same solutions as in figure 1 ($P = 0.1$).

evident that the mean flow energy is always only a small fraction of the energy of the fluctuating velocity field. For $Q = 0$ the restricted and the unrestricted cases of mean flows give rather different results since the component $U_1 \sin \pi(z+\frac{1}{2})$ dominates in the unrestricted case. As the magnetic field strength increases the component $U_3 \sin 3\pi(z+\frac{1}{2})$ becomes the main contributor to the mean flow and the energies in the restricted and unrestricted cases move closer. Usually the sign of the coefficient U_3 is such that the mean flow in the centreplane of the layer is directed in the direction of wave propagation.

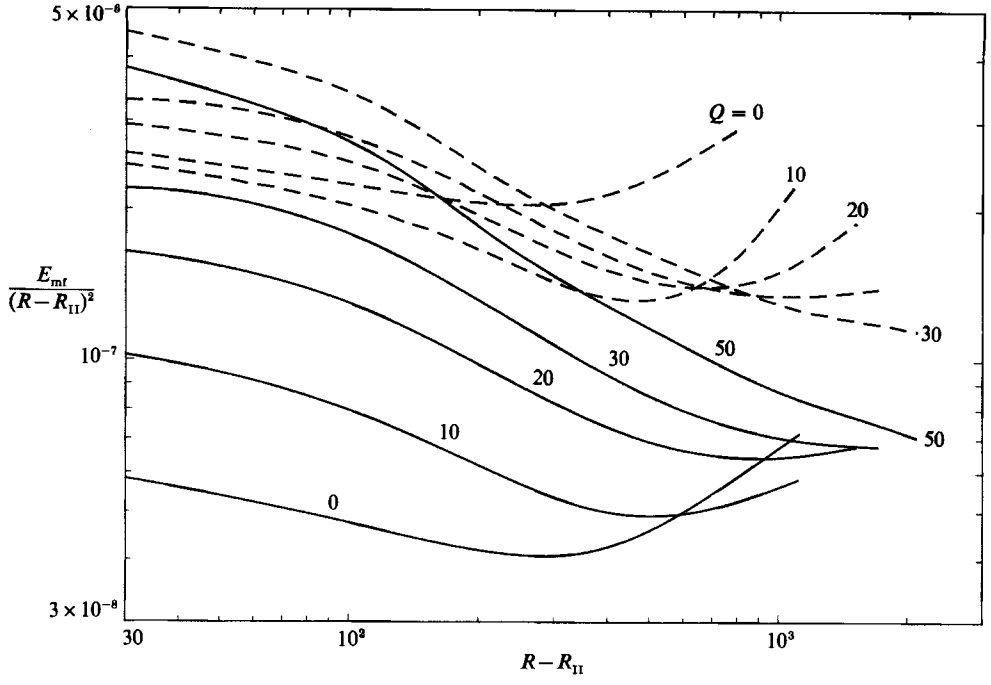

FIGURE 12. As figure 11, but for the same solutions as in figure 2 ($P = 0.025$).

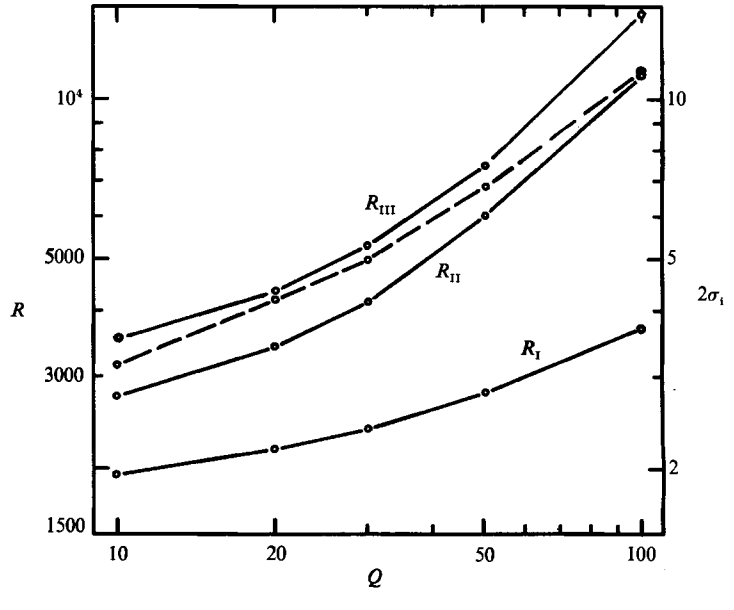

FIGURE 13. The Rayleigh numbers R_I, R_{II}, R_{III} (left ordinate) and the frequency σ_i (dashed line, right ordinate) of the asymmetric wave instability relative to the reference frame drifting with the travelling waves in case of restricted mean flow. The results obtained for the cases of figure 1 are indicated by the circles and have been connected by straight lines for better visualization.

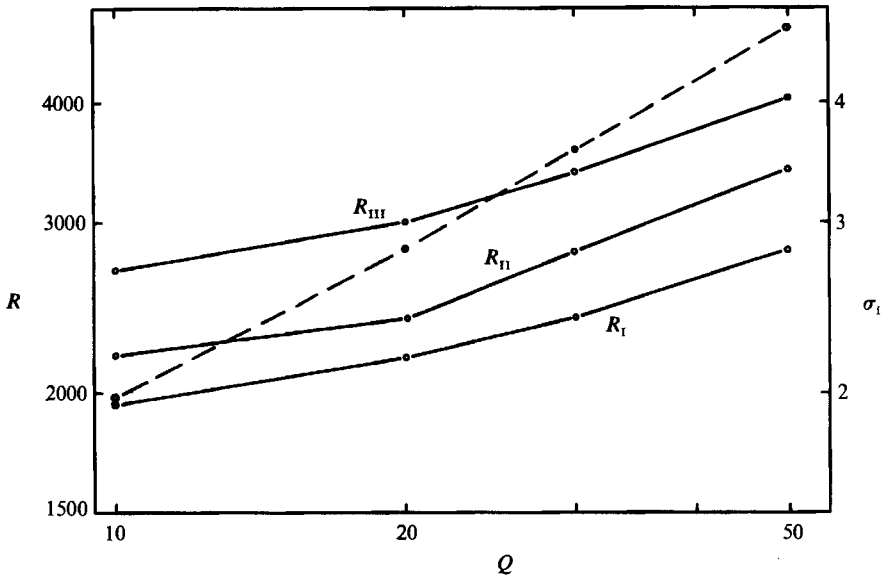

FIGURE 14. Same as figure 13 but for the cases of figure 2.

	$P = 0.71$ $\alpha_y = 2.2$			$P = 0.1$, $\alpha_y = 2.6$			$P = 0.025$, $\alpha_y = 2.9$		
α_x	2.0	2.3	2.6	1.9	2.2	2.5	1.9	2.2	2.5
R_{III}(u)	11473		8351	3236	2801	2778	2510	2973	2415
σ_i(u)	17.57		9.58	5.73	5.02	5.34		2.99	1.69
R_{III}(r)	10679	9384	7965	2977	2707	2710	2561	2482	2334
σ_i(r)	16.04	12.09	9.18	4.65	4.39	4.67		1.59	1.47

TABLE 1. Rayleigh numbers R_{III} and imaginary parts σ_i of growth rates for the onset of asymmetric oscillation for $Q = 0$

4. The stability of travelling-wave convection

The stability of convection in the form of travelling waves has been studied in CB as a function of the Prandtl number. The additional influence of the vertical magnetic field does not affect the nature of the instability. Only the Rayleigh number R_{III} for the onset of asymmetric waves is increased by roughly the same relative amount by which R_{II} is increased with increasing Q. This property is evident in figures 13 and 14 which display the transition Rayleigh numbers for $P = 0.1$ and $P = 0.025$. These figures also show the second frequency which characterizes the asymmetric wave component. This frequency σ_i is computed relative to the moving frame of reference with respect to which the symmetric travelling-wave convection is stationary. Only the case of restricted mean flow has been used in plotting R_{III}. As Q increases, the values R_{III} and σ_i for the case of unrestricted flow differ imperceptibly from those in the restricted case.

For $Q = 0$ the Rayleigh number R_{III} for onset of asymmetric oscillations and the corresponding frequency σ_i are given in table 1 for different combinations of the wavenumbers α_y and α_x characterizing travelling-wave convection. Values for both restricted and unrestricted mean flow have been listed. The difference is larger than

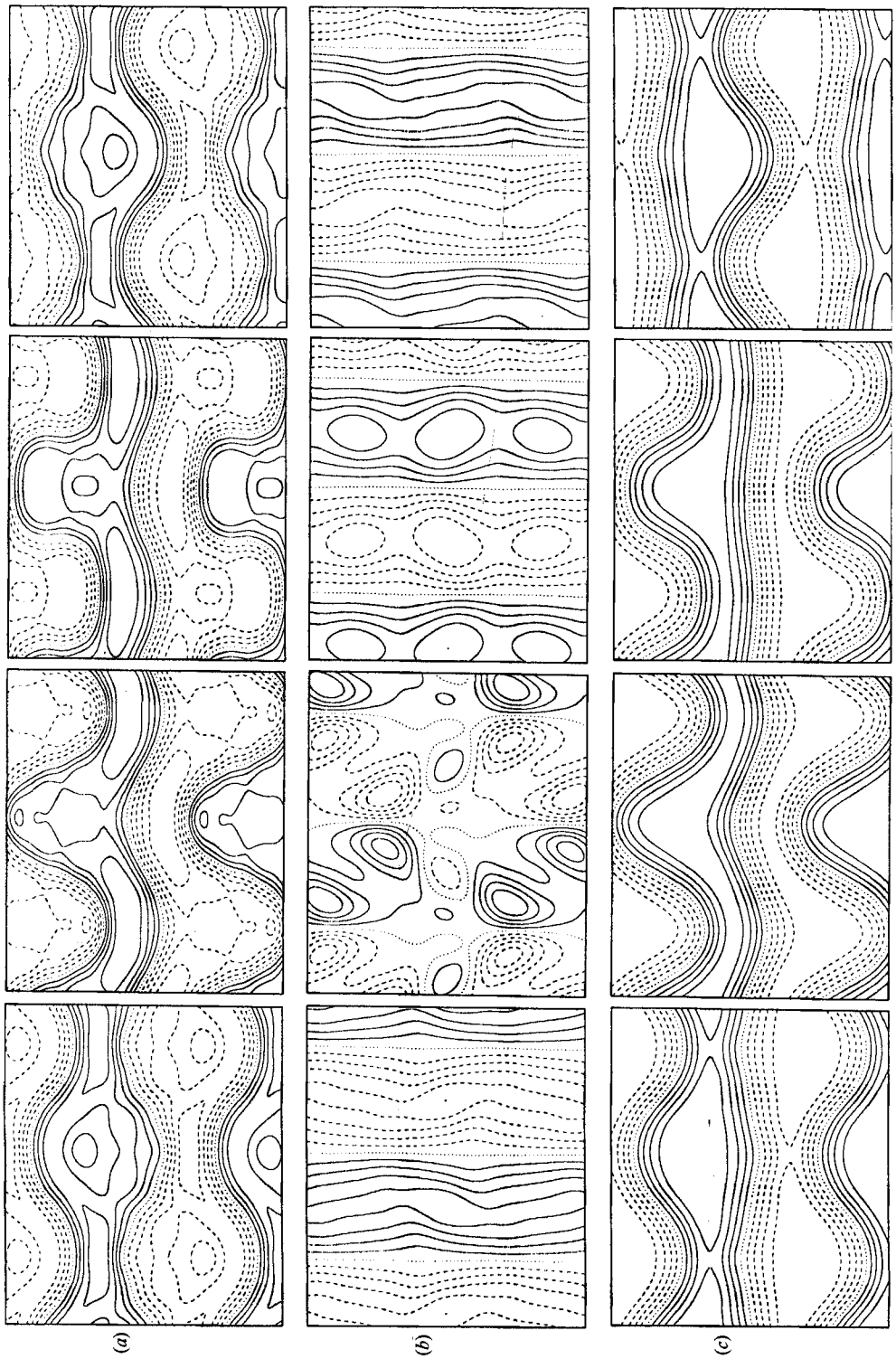

FIGURE 15. Asymmetric standing oscillations for $P = 0.1$, $R = 3500$, $Q = 0$, $\alpha_z = 2.2$, $\alpha_y = 2.6$ with unrestricted mean flow. The vertical velocity at $z = 0$, the function ψ at $z = 0$ and the vertically averaged temperature $\bar{\theta}$ are shown in rows (*a*), (*b*) and (*c*) respectively, at four times separated by $\Delta t = 0.16$, increasing from left to right. The total time span $3\Delta t$ corresponds to about one half-period of the oscillation.

for the finite values of Q plotted in figures 13 and 14, but seldom exceeds 5%. Although the mean flow in either case has very little influence on the other properties of travelling-wave convection, in the case of air the onset of asymmetric oscillations depends rather sensitively on it. For this reason the case $P = 0.71$ has been included in the table.

The mean flow has a stabilizing influence on the onset of asymmetric oscillations in general. The values of R_{III} are thus higher in the unrestricted case than in the restricted case and agree quite well in the latter case with those of table 2 of CB which have been computed without inclusion of a mean flow. The only exception appears to be in the case of air for $\alpha_x = 2.0$, where the value for the unrestricted flow seems to match the earlier value best. In this comparison it must be taken into account, however, that $N_{\mathrm{T}} = 8$ was used in the computations of R_{III} in CB, while $N_{\mathrm{T}} = 10$ has been used in the present computations. There is another exceptional case included in table 1 which occurs for $P = 0.025$, $\alpha_x = 1.9$. A monotonic asymmetric instability with vanishing σ_{i} precedes the onset of asymmetric oscillations in this case when $N_{\mathrm{T}} = 10$ is used in the computations, while for $N_{\mathrm{T}} = 8$ the oscillating instability comes first. But since this phenomenon occurs only for the rather low wavenumber $\alpha_x = 1.9$ no special attention has been devoted to it at this point.

The solution bifurcating from the travelling-wave solution in the case of the asymmetric wave instability can no longer be described as a steady solution with respect to a suitable frame of reference. An integration in time of the basic equation is required for the description of the bifurcating form of convection. This time integration can be carried out by assuming that the coefficients $\hat{a}_{lm}$, etc. in (2.5) are functions of time. Solutions of this kind have been described in CB for the case of $P = 0.71$. They are hardly changed by the effects of a mean flow. Instead of the asymmetric travelling solution in air, however, a standing asymmetric oscillation develops when the Prandtl number is lowered. Figure 15 shows a typical example in the case $P = 0.1$. The travelling-wave component has virtually disappeared and the convection velocity field is essentially symmetric with respect to certain planes $x =$ const. The frequency of oscillation corresponds to $\sigma_{\mathrm{i}} + \omega$, where σ_{i} is the imaginary part of the growth rate of the asymmetric instability and ω is the frequency of the travelling waves. The Nusselt number varies by about 20% throughout the cycle, but the time-averaged value does not differ much from the steady value of symmetric travelling waves. Because of the rather long time integrations that are necessary to reach a reasonably stationary state it becomes computationally expensive to obtain accurate solutions. No systematic study of the parameter dependence of standing asymmetric oscillations has yet been done.

5. Concluding remarks

In the limit of high magnetic diffusion that has been assumed in the present analysis, and which is typical for convection in liquid metals, the equation of magnetic induction gives rise to an additional linear term in the equation of motion which resembles the viscous friction term according to equations (2.3*d*, *e*). In this sense the parameter Q increases the effective viscosity and thereby increases the effective Prandtl number and decreases the effective Rayleigh number. The Rayleigh number for the onset of convection rolls is thus increased and the nonlinear properties of the problem resemble those of a larger-Prandtl-number fluid with a lower or vanishing value of Q. For this reason the onset of the oscillatory instability

is even more delayed than the onset of convection and the same can be said for the onset of the asymmetric waves.

While this reasoning explains the general similarity of the curves for different values of Q shown in figures 1, 2, 6, and 7, it is only roughly correct. Because the differential operators multiplied by Q in (2.3) are different from the friction operators, a growing magnetic field strength leads to an increase of the wavenumber α. There is also a qualitatively new effect in the form of the subcritical onset of finite-amplitude travelling waves which appears to be absent for small or vanishing values of Q. The imposition of a vertical magnetic field thus leads to some novel effects which cannot easily be anticipated from the non-magnetic limit $Q = 0$.

We have already mentioned in the preceding section the monotonous mode of the asymmetric wave instability which is characterized by $\sigma_1 = 0$. Even in those cases where the growth rate of the mode with $\sigma_1 = 0$ is always less than that for the mode with $\sigma_1 \neq 0$, we find that the Rayleigh numbers for the onset of these two modes approach each other as Q is increased. It is thus possible that the new instability may enter the picture for sufficiently large values of Q. It may also be favoured at lower values of the Prandtl number. A similar phenomenon is observed for travelling waves in the presence of a horizontal magnetic field where it is more accessible to numerical computations. We therefore shall return to this instability in future work on the effect of a horizontal magnetic field on travelling-wave convection.

The support of Geophysics and Atmospheric Science Sections of the US National Science Foundation for the research reported in this paper is gratefully acknowledged.

REFERENCES

BUSSE, F. H. 1972 The oscillatory instability of convection rolls in a low Prandtl number fluid. *J. Fluid Mech.* **52**, 97–112.

BUSSE, F. H. & CLEVER, R. M. 1982 On the stability of convection rolls in the presence of a vertical magnetic field. *Phys. Fluids* **25**, 931–935.

BUSSE, F. H. & FRICK, H. 1985 Square-pattern convection in fluids with strongly temperature-dependent viscosity. *J. Fluid Mech.* **150**, 451–465.

CHANDRASEKHAR, S. 1961 *Hydrodynamic and Hydromagnetic Stability* Clarendon.

CLEVER, R. M. & BUSSE, F. H. 1974 Transition to time-dependent convection. *J. Fluid Mech.* **65**, 625–645.

CLEVER, R. M. & BUSSE, F. H. 1987 Nonlinear oscillatory convection. *J. Fluid Mech.* **176**, 403–417.

FAUVE, S., BOLTON, E. W. & BRACHET, M. E. 1987 Nonlinear oscillatory convection: A quantitative phase dynamics approach. *Physica* **29 D**, 202–214.

FAUVE, S., LAROCHE, C., LIBCHABER, A. & PERRIN, B. 1984 Chaotic phases and magnetic order in a convective fluid. *Phys. Rev. Lett.* **52**, 1774–1777.

LIBCHABER, A., FAUVE, S. & LAROCHE, C. 1983 Two-parameter study of the routes to chaos. *Physica* **7 D**, 73–84.

PROCTOR, M. R. E. & WEISS, N. O. 1982 Magnetoconvection. *Rep. Prog. Phys.* **45**, 1317–1379.